AIP | Physics of Plasmas

Temporal modulation of plasma species in atmospheric dielectric barrier discharges

Aijun Yang, Xiaohua Wang, Dingxin Liu, Mingzhe Rong, and Michael G. Kong

Citation: Physics of Plasmas (1994-present) **21**, 073507 (2014); doi: 10.1063/1.4890481
View online: http://dx.doi.org/10.1063/1.4890481
View Table of Contents: http://scitation.aip.org/content/aip/journal/pop/21/7?ver=pdfcov
Published by the AIP Publishing

Articles you may be interested in

Ultraviolet-B radiation enhancement in dielectric barrier discharge based xenon chloride exciplex source by air
Appl. Phys. Lett. **105**, 013505 (2014); 10.1063/1.4887379

Direct current dielectric barrier assistant discharge to get homogeneous plasma in capacitive coupled discharge
Phys. Plasmas **21**, 063506 (2014); 10.1063/1.4882442

Measurement of OH (X 2) in immediate vicinity of dielectric surface under pulsed dielectric barrier discharge at atmospheric pressure using two geometries of laser-induced fluorescence
J. Appl. Phys. **115**, 133302 (2014); 10.1063/1.4870598

Columnar discharge mode between parallel dielectric barrier electrodes in atmospheric pressure helium
Phys. Plasmas **21**, 013503 (2014); 10.1063/1.4861608

Plasma formation in atmospheric pressure helium discharges under different background air pressures
Phys. Plasmas **19**, 093506 (2012); 10.1063/1.4754516

This article is copyrighted as indicated in the article. Reuse of AIP content is subject to the terms at: http://scitation.aip.org/termsconditions. Downloaded to IP: 117.32.153.177 On: Fri, 19 Sep 2014 02:45:44

Temporal modulation of plasma species in atmospheric dielectric barrier discharges

Aijun Yang,[1,a)] Xiaohua Wang,[1,a),b)] Dingxin Liu,[1] Mingzhe Rong,[1,b)] and Michael G. Kong[1,2,3]
[1]*Centre for Plasma Biomedicine, State Key Laboratory of Electrical Insulation and Power Equipment, Xi'an Jiaotong University, Xi'an 710049, People's Republic of China*
[2]*Frank Reidy Research Center for Bioelectrics, Department of Electrical and Computer Engineering, Old Dominion University, Virginia 23508, USA*
[3]*Department of Electrical and Computer Engineering, Old Dominion University, Norfolk, Virginia 23529, USA*

(Received 26 April 2014; accepted 7 July 2014; published online 17 July 2014)

The atmospheric pressure dielectric barrier discharge in helium is a pulsed discharge in nature and the moment of maximum species densities is almost consistent with peak discharge current density. In this paper, a one-dimensional fluid model is used to investigate the temporal structure of plasma species in an atmospheric He-N_2 dielectric barrier discharge (DBD). It is demonstrated that there exist microsecond delays of the moments of the maximum electron and ion densities from the peak of discharge current density. These time delays are caused by a competition between the electron impact and Penning ionizations, modulated by the N_2 level in the plasma-forming gas. Besides, significant electron wall losses lead to the DBD being more positively charged and, with a distinct temporal separation in the peak electron and cation densities, the plasma is characterized with repetitive bursts of net positive charges. The temporal details of ionic and reactive plasma species may provide a new idea for some biological processes. © *2014 AIP Publishing LLC*.
[http://dx.doi.org/10.1063/1.4890481]

I. INTRODUCTION

Dielectric barrier discharges, often known as DBDs, are a common route to nonequilibrium plasmas at elevated gas pressures.[1] At atmospheric pressure, DBDs usually operate in a filamentary mode consisting of a large number of randomly occurring microdischarges (i.e., short-lived streamer filaments). Localized heat deposition of these plasma filaments and their lack of temporal repetitiveness restrict the application scope of atmospheric pressure DBDs, particularly for those that require controlled or even uniform treatment.[1–3] However, technology advances over the past 20 yr or so have made it possible to realize spatially homogeneous and temporally repetitive DBDs at atmospheric pressure in specific parametric ranges of the gas mixture, the excitation frequency or a pulsed excitation.[1–7] Homogeneous barrier discharges are of great interest for controlled, reproducible treatment of solid and liquid materials including living tissue and soft matters.[4–8]

Homogeneous atmospheric pressure DBDs have been investigated both experimentally and numerically, and their current understanding is extensive particularly in gas mixtures dominated by noble gases (e.g., helium and argon).[1,9–14] Reaction chemistry, central to almost all plasma applications, tends to be studied by means of its dependence upon time-averaged densities of plasma species and the relative chemical composition of the latter in the ionized gas as the discharge conditions are varied, even though it is known that different plasma species may reach their maximum concentrations at different times.[12] This is appropriate for most existing applications in which differences in temporal profiles of plasma species have little consequence to the treatment efficacy of samples, for example, those with properties insensitive to short-term details of incoming plasma species such as packaging plastics, metallic tools, and contaminated environment. However, new and emerging applications of atmospheric pressure plasmas, such as those involving living systems[7] and nanoscale systems,[17] invite a revisit to the conventional strategy of relying on time-averaged densities of reactive plasma species.

N_2 impurity is known to strongly influence the level of ionization in helium DBDs and, to a lesser extent, the temporal features of the discharge current. For example, Golubovskii and co-worker showed that the impurities of N_2 in helium could influence the symmetry of the discharge current.[14] Yuan and co-workers found that without the presence of N_2 impurities in the plasma chemistry model, the multipulse phenomena at lower frequencies cannot be simulated accurately since the pure helium chemistry model results in single broad pulse at the lower frequencies.[15] Martens and coworkers have demonstrated how nitrogen may strongly alter the ionic composition of atmospheric pressure He plasma and indeed the temporal features of the discharge current.[16,17] Urabe and co-workers found that the ionization frequency is maximized under the 0.25% condition of the N_2 impurity ratio.[18] Of particular note is a recent report of an atmospheric He-N_2 DBD with N_2 fixed at 100 ppm,[19] in which a delay of a few μs in the N_4^+ concentration from other species was observed. Recently, there have been also several experimental

[a)]A. Yang and X. Wang contributed equally to this work.
[b)]Authors to whom correspondence should be addressed. Electronic addresses: xhw@mail.xjtu.edu.cn and mzrong@mail.xjtu.edu.cn.

 © 2014 AIP Publishing LLC

This article is copyrighted as indicated in the article. Reuse of AIP content is subject to the terms at: http://scitation.aip.org/termsconditions. Downloaded to IP: 117.32.153.177 On: Fri, 19 Sep 2014 02:45:44

works exploring the time-evolution of ionic species in an atmospheric pressure helium discharge[20–22] and similar phenomenon is found in these studies. This observation was not explained in terms of plasma physics nor explored for its existence for other plasma species. The perhaps of greater interest is whether the phenomenon is a detail of DBD physics with no practical relevance or whether it may broaden how DBDs are used to treat biotic materials as well as smart materials,[23] particularly those strongly sensitive to short-term temporal details of external stimuli. It is worth noting that the above-mentioned microsecond delay of the peak N_4^+ density falls within the nanosecond-millisecond timescale of some biomolecular and cellular processes such as ligand binding, protein folding, and enzymatic catalysis.[24–26]

Our study first investigates temporal characters of plasma particle concentrations of He-N_2 DBDs and their modulation by the nitrogen admixture in terms of time delays in the moments of the maximum concentrations of charged and neutral plasma species from the instant of the peak discharge current density by means of a fluid modelling. Following a short introduction to the numerical method and details of relevant chemical reactions in Sec. II, the results of the study are presented and discussed in Sec. III for a wide N_2 content from 0.1 to 10 000 ppm so as to bring out a full scope of temporal modulation of plasma chemistry. Finally, our findings are summarised in Sec. IV.

II. COMPUTATIONAL MODEL

The present study considers an atmospheric pressure He-N_2 DBD sustained at nominally 10 kHz and a peak applied voltage of 1 kV between two dielectrically insulated electrodes. The relative permittivity of the dielectric insulation layers is 9 and the thickness of each layer is 1 mm. The gas gap is fixed at 2 mm and the gas temperature at 300 K. The amount of nitrogen in the plasma-forming gas varies from 0.1 to 10 000 ppm. A one-dimensional fluid model is employed here, following its successful simulation of atmospheric pressure helium plasmas.[27–29] Details of the model are given in the literature, however a brief summary of its key features is provided here. The very high particle collision frequency at the atmospheric pressure allows the usage of drift and diffusion approximation. The governing equations of the fluid model are given below

$$\frac{\partial n_i}{\partial t} + \nabla \cdot \mathbf{\Gamma}_i = S_i \qquad \mathbf{\Gamma}_i = \mathrm{sgn}(q_i) n_i \mu_i \mathbf{E} - D_i \nabla n_i, \tag{1}$$

$$\frac{\partial n_e \varepsilon}{\partial t} + \frac{5}{3}\nabla \cdot (\varepsilon \mathbf{\Gamma}_e - n_e D_e \nabla \varepsilon) = -e\mathbf{\Gamma}_e \cdot \mathbf{E} - \sum_j \Delta E_j R_j - 3\frac{m_e}{m_{He}} R_{el} k_B (T_e - T_{He}), \tag{2}$$

$$\varepsilon_0 \nabla \cdot \mathbf{E} = \sum_i q_i n_i, \tag{3}$$

where n_i, $\mathbf{\Gamma}_i$, S_i, q_i, μ_i, and D_i represent, respectively, the particle density, flux, net generation rate, charge, mobility, and diffusion coefficients for plasma species i. $\mathbf{E}$ is the electric field and $\varepsilon = 1.5 k_B T_e$ is the mean electron energy. ε_0 is the vacuum permittivity, e is the elementary charge, and k_B is the Boltzmann constant. R_{el} is the momentum transfer collisional rate between electrons and helium, T_e is the temperature of electron and T_{He} is the temperature of helium. ΔE_j and R_j are the electron energy loss due to inelastic collision j and its corresponding reaction rate. Subscript e represents electron. Equations (1)–(3) are solved by using a time-dependent finite-element partial differential equation solver, COMSOL Multiphysics, and simulation results are post-processed with MATLAB.[27–29]

For charged particle fluxes to the dielectrics, the following boundary conditions are used:

$$\mathbf{\Gamma}_e \cdot \mathbf{n} = -\alpha \mu_e \mathbf{E} \cdot \mathbf{n} n_e + 0.25 v_{th,e} n_e - \gamma \sum_p \mathbf{\Gamma}_{+,p}, \tag{4}$$

$$\mathbf{\Gamma}_+ \cdot \mathbf{n} = \alpha \mu_+ \mathbf{E} \cdot \mathbf{n} n_+ + 0.25 v_{th,+} n_+, \tag{5}$$

where $\mathbf{n}$ is the normal vector pointing towards the dielectric. v_{th} is the thermal velocity and γ is the secondary emission coefficient. γ is set at 0.05 for helium ions and 0.001 for nitrogen ions.[19] The switching function α takes the value of 1 when the drift velocity is directed towards the electrodes and zero, otherwise

$$\alpha = \begin{cases} 1, & \mathrm{sgn}(q_i)\mu_i \mathbf{E} \cdot \mathbf{n} > 0 \\ 0, & \mathrm{sgn}(q_i)\mu_i \mathbf{E} \cdot \mathbf{n} \le 0. \end{cases} \tag{6}$$

For neutral species, the boundary conditions are

$$\mathbf{\Gamma}_i \cdot \mathbf{n} = 0.25 v_{th} n_i. \tag{7}$$

For simplicity, the mean electron energy at both gas-facing borders of the electrodes is fixed at 1 eV. For the Poisson equation, one electrode is grounded and a sinusoidal voltage is applied to the other electrode. The gas-dielectric interface has the following boundary condition:

$$\varepsilon_{dielectric} \mathbf{E} \cdot \mathbf{n} - \varepsilon_0 \mathbf{E} \cdot \mathbf{n} = \sigma, \tag{8}$$

where $\varepsilon_{dielectric}$ is the permittivity of dielectric and σ is the surface charge density on the dielectric. Similar to previous study,[16] the model comprises 9 species (He, e, He^+, He_2^+, He*, He_2*, N_2, N_2^+, and N_4^+) and 18 chemical reactions. The ions N^+ and N_3^+ and the neutral species N, N*, and N_2* are not taken into account for matters of simplicity. N^+ and N_3^+ are very quickly converted into N_2^+ through $N^+ + N + He \rightarrow N_2^+ + He$ and $N_3^+ + N \rightarrow N_2^+ + N_2$,[16] respectively. N* and N_2* are of minor importance in the charged species composition of He-N_2 discharge, as the N_2 impurity level is very low in this study. The chemical reactions used in the model are obtained from most of the publications on He-N_2 discharge. Overall, the species and chemical reactions considered in this paper are sufficient to provide an accurate representation of the He-N_2 discharge chemistry based on the previous studies.[14–17] The reaction rate coefficients for electron impact reactions as well as the transport coefficients of electron were calculated using an offline Boltzmann solver

This article is copyrighted as indicated in the article. Reuse of AIP content is subject to the terms at: http://scitation.aip.org/termsconditions. Downloaded to IP: 117.32.153.177 On: Fri, 19 Sep 2014 02:45:44

BOLSIG+.[31] The remaining reactions rate coefficients were obtained from Ref. 16. The transport coefficients for other species are obtained from the literature.[27,32]

III. RESULTS AND DISCUSSIONS

A. Time delays

For all results represented here, the He-N_2 DBD is operated at sufficiently low current densities such that there is one discharge event every half cycle of the applied voltage. Simulation results suggest that the pulse shape of the discharge current density remains little changed and its pulsewidth is less than 1 μs (more specifically $\Delta t_c = 0.25$–$0.36\,\mu$s for $[N_2] = 10$–100 ppm and $\Delta t_c = 0.99\,\mu$s for $[N_2] = 1000$ ppm, data not shown). The narrowness of the current pulse allows for the instant of the peak current density to be used as the reference point to which time delays of the maximum particle concentrations are calculated and considered.

Fig. 1 illustrates the space-averaged electron density as a function of time at four N_2 content levels of $[N_2] = 10$, 30, 100, and 1000 ppm. The zero point of the horizontal axis represents the moment of the maximum discharge current density. At 10 ppm, the electron density reaches its maximum value close to $t = 0$ and its curve has a singular peak hereafter known as PV1. This is consistent with the results of numerical studies reported in literature.[33] Increase in the N_2 content level leads to a reduction in PV1 and a rise of the tail of the electron density curve. At 30 ppm, the electron density is seen to possess two peaks with the first being narrow and the second being broad in pulse shape. The second peak, hereafter referred to as PV2, has the same magnitude as PV1 and lags the peak current density by $\Delta t_e = 5.8\ \mu$s, almost 20 times as large as the pulse width of the current density at 30 ppm. As the nitrogen level is increased further, PV2 becomes increasingly dominant with concurrent reduction in the magnitude of PV1. Above 100 ppm as seen in the 1000 ppm case, the first peak is no longer distinguishable. The existence of two electron density peaks has not been reported before nor has the considerable time delay of the second electron density peak. Interestingly, such temporal features can be modulated by the N_2 content.

Most plasma species in the discharge plasma are directly or indirectly linked to electrons. Therefore, the time delay of the maximum electron density from the peak current density should be reflected in the concentrations of neutral and other charged plasma species. The time delays of space-averaged concentrations of charged particles and helium metastables from the instant of the maximum current density are shown in Fig. 2 as a function of the N_2 content. It is evident that the time lags for nitrogen cations and electrons are significant, with the maximum delay at, respectively, $\Delta t_{N2+} = 12\,\mu$s, $\Delta t_{N4+} = 11.1\,\mu$s, and $\Delta t_e = 5.8\,\mu$s. Consistent with previous reports,[16] our simulation shows that, when compared in space- and time-averaged concentrations, the nitrogen cations become dominant when the N_2 level is above 1 ppm (data not shown). For $[N_2] = 1$–30 ppm, N_2^+ ions are found to dominate, with a time lag of 1.9–12 μs from the peak current density. Xiong *et al.*[20] also found that the peak moment of excited N_2^+ (B, $v' = 0$) by optical emission spectroscopy is delayed by about tens of ns compared with that of discharge current in a helium plasma jet. It is apparent that the time delay of excited N_2^+ (B, $v' = 0$) is much smaller than that of N_2^+ in this paper. While Oh *et al.*[21] and McKay *et al.*[22] found that the time delays for N_2^+ and O_2^+ are a few μs by a mass/energy analyzer HPR60. On the other hand, the electron density has a negligible time delay for 0–30 ppm. So the electrons reach their maximum space-averaged concentration earlier than the cations and the duration of 1.9–12 μs, for 1–30 ppm, represents a timescale when the electrical neutrality of the plasma may not be maintained.

Above 30 ppm in N_2 impurity, N_4^+ becomes the dominant cations when compared in terms of space- and time-averaged concentrations (data not shown). The delay of the instant of its maximum concentration is seen to decrease monotonically from $\Delta t_{N4+} = 8\,\mu$s at $[N_2] = 30$ ppm. The instant of the maximum electron density is seen in Fig. 2 to jump to $\Delta t_e = 5.8\,\mu$s at $[N_2] = 30$ ppm, and then to undergo a similar monotonic decay to the N_4^+ density. However, the

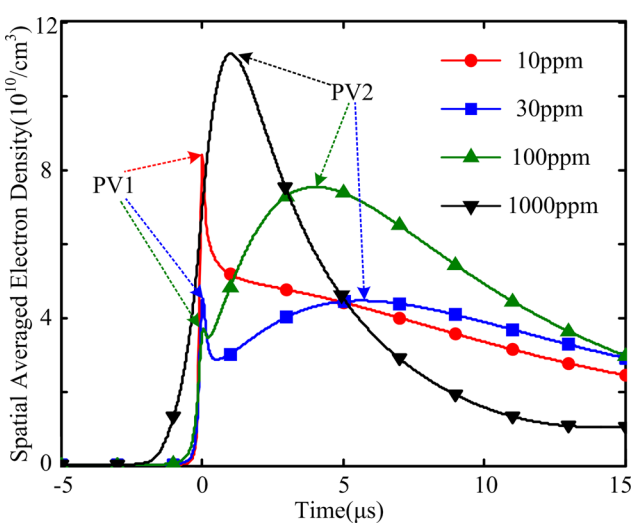

FIG.1. Space-averaged electron density as a function of time at different N_2 levels.

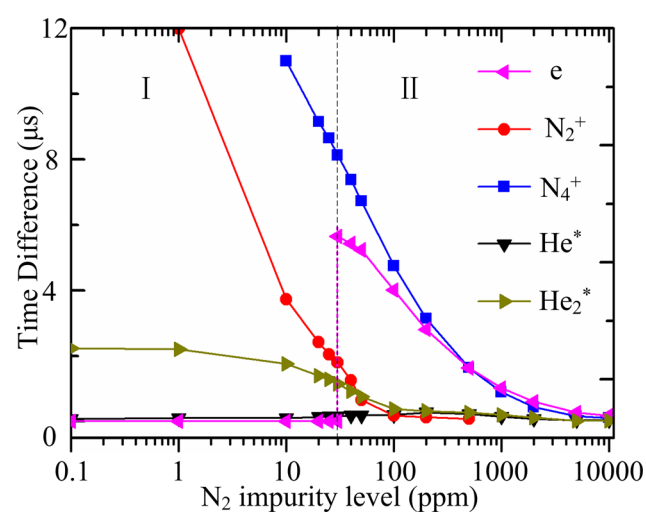

FIG. 2. Time lags of the peak space-averaged particle densities from the peak current density as a function of the N_2 content.

This article is copyrighted as indicated in the article. Reuse of AIP content is subject to the terms at: http://scitation.aip.org/termsconditions. Downloaded to IP: 117.32.153.177 On: Fri, 19 Sep 2014 02:45:44

N_4^+ density has a greater decay rate between 30 and 300 ppm, and its time delay becomes similar to that of electrons after $[N_2] = 300$ ppm. In other words, the relative time delay between electron and cation concentrations may disappear around 300 ppm. The above discussion suggests that the nitrogen content in the plasma-forming gas may be adjusted to tune the temporal profile of the net-charge density and hence the electrical neutrality of the DBD. It is worth mentioning also that helium ions have a time delay much less than 0.3 μs (not shown in Fig. 2).

The point of $[N_2] = 30$ ppm appears to be a separation of two regions. In the first region (indicated by "I" in Fig. 2) below 30 ppm, the time delay for electrons is no more than 0.1 μs and almost constant. Above 30 ppm in the second region (indicated by "II" in Fig. 2), the time delay of the instant of the peak electron density has a step increase to $\Delta t_e = 5.8$ μs, much greater than the current density pulse of 0.30–0.36 μs for $[N_2] = 30$–100 ppm. The monotonic decay with $[N_2]$ in the instant of the peak electron density after 30 ppm is also seen in the trends for He_2*, N_2^+, and N_4^+ species. For $[N_2]$ above 300 ppm, the time difference for $N_2^+$and He_2* is not more than 0.3 μs. Above 5000 ppm, the time delays for all species are not more than 0.3 μs. To gain insights into possible mechanisms responsible for the time delays, space-averaged electron generation, and loss rates are shown in Fig. 3 for three N_2 content levels at 10, 100, and 1000 ppm. Identical to that in Fig. 1, the time zero point is the moment of the maximum current density and the vertical dashed line corresponds to the moment of the maximum space-averaged electron density. The electron density reaches its maximum when the electron loss rate exceeds the electron generation rate. The main route for electron loss is the wall loss at the electrodes, and their recombination with ions is comparably negligible. In other words, the electron loss remains relatively independent of the nitrogen content in the plasma-forming gas. By contrast, electron generation is dominated by the electron impact ionization and the Penning ionization with the relative importance of the latter determined by the N_2 level. Penning ionization includes self-Penning ionization of helium metastables and ionization of N_2 by helium metastables. Our simulation indicates that for $[N_2] > 10$ ppm the rate of self-Penning ionization is negligible compared to that of Penning ionization of nitrogen molecules. As our discussion of Figs. 1 and 2 is largely for 10–10 000 ppm, self-Penning ionization will be ignored hereafter and the term of Penning ionization used specifically for the ionization of N_2 by He metastables.

Fig. 3 shows that the self-Penning ionization has a very low rate for all nitrogen contents considered. It is seen in Fig. 3(a) that the electron impact ionization is dominant at $[N_2] = 10$ ppm that is too small for the Penning ionization to significantly contribute to electron generation. Shortly after $t = 0$, the rate of electron impact ionization starts to decline and the electron loss rate exceeds its generation rate at point PV1*(or $t = 0.03$ μs), resulting in the maximum space-averaged electron density PV1 in Fig. 1.

With N_2 content increased to 100 ppm, the Penning ionization of N_2 becomes stronger and its duration becomes longer (data not shown), leading to an increasingly more significant contribution. These combine to result in the second peak of the electron density (i.e., PV2) in Fig. 1. At $[N_2] = 100$ ppm in region II (see Fig. 2), Fig. 3(b) shows that the electron generation rate due to the Penning ionization of N_2 is comparable to that of the electron impact ionization for $t < 0.2$ μs but becomes dominant after $t = 0.2$ μs. As both helium metastables and nitrogen molecules persist for a long period of time, Penning ionization last for a long period of time, leading to a very large time delay for the peak electron density at 100 ppm. Further increase of N_2 content to 1000 ppm in region II, the Penning ionization is so strong that PV1* is no longer present in Fig. 3(b) and so the electron density has no PV1 above 100 ppm in Fig. 3. It is worth noting that the Penning ionization is dominant at

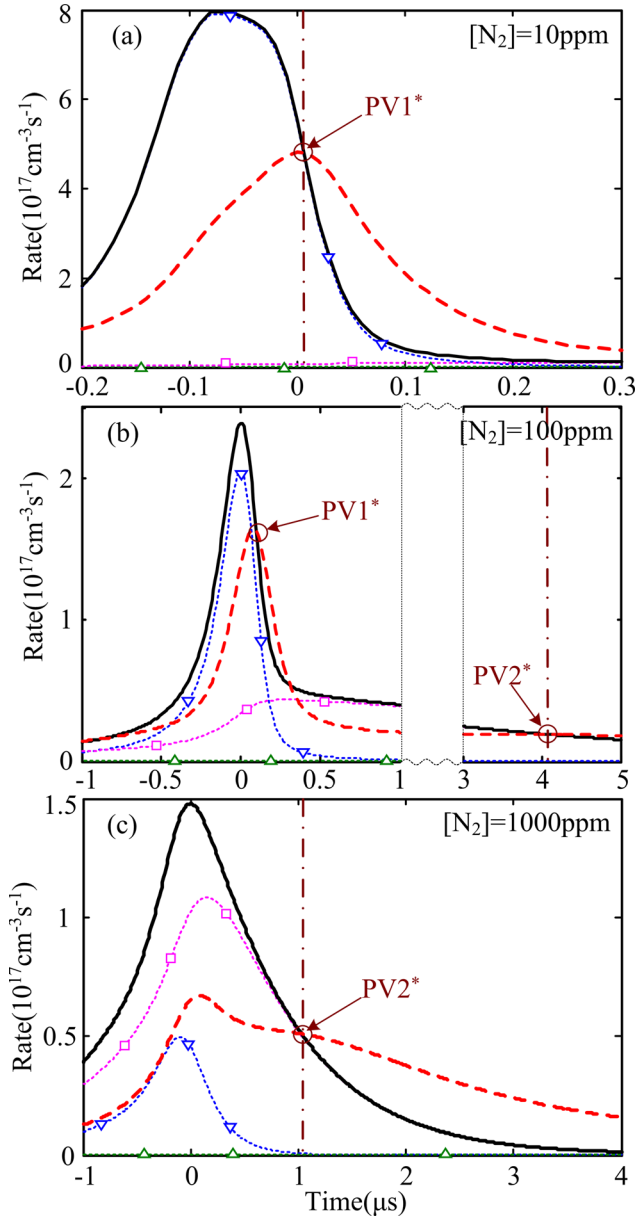

FIG. 3. Space-averaged rates of electron generation (- - -) and electron loss (—) as a function of time. Electron loss is via electron impact ionization (- -▽- -), Penning ionization of N_2 (- -□- -) and self-Penning ionization of He metastables (- -△- -). The vertical dotted dashed line is when the electron density is maximum.

This article is copyrighted as indicated in the article. Reuse of AIP content is subject to the terms at: http://scitation.aip.org/termsconditions. Downloaded to IP: 117.32.153.177 On: Fri, 19 Sep 2014 02:45:44

1000 ppm (see Fig. 3(c)). PV2* in Fig. 3(c) is about 1 μs behind the maximum moment of discharge current density, consistent with the time difference for the electron density at 1000 ppm.

It is therefore clear that PV1 of the electron density is mainly caused by the electron impact ionization and PV2 by the Penning ionization of N_2. The electron impact ionization occurs mainly during electron multiplication and as such the moment of PV1 is very close to that of the maximum discharge current density. On the other hand, an increment in the N_2 content first enhances the strength of Penning ionization of N_2 and therefore the electron density. At a high N_2 content, Penning ionization of N_2 becomes very active and this leads to an efficient exhaust of helium metastables, thus causing a reduction in the duration of Penning ionization. In turn, this results in a premature maximum of the electron density close to $t = 0$ or the instant of PV2 shifting towards $t = 0$. These are shown in Figs. 1 and 3(c). As $[N_2]$ is raised to 5000 ppm, the delay of the instant of the peak electron density becomes negligible as shown in Fig. 2.

It is worth supporting the above discussion from the standpoint of He metastables and their production and loss. In both regions with $[N_2]$ spanning for 10–10 000 ppm, $e + He \rightarrow e + He^*$ is responsible for the generation of He* and this reaction mainly occurs during the gas breakdown process. Time delay for He* from the instant of the peak current density is negligible for all N_2 levels. For $[N_2] < 1$ ppm, the Penning ionization is too weak to contribute to any sizeable reduction of He_2^*. Therefore, time delay for He_2^* shows little dependence on N_2 impurity (data not shown). With increasing $[N_2]$, Penning ionization becomes progressively dominant in the reduction of He_2^*, leading to an increasingly early onset of its peak concentration. In general, the time delay for He_2^* is negligible for $[N_2] \geq 100$ ppm. The little time delay of He* and the enhanced reduction of He_2^* for $[N_2] \geq 100$ ppm contribute to the reduced time delay of the peak electron density above 100 ppm (see Figs. 1 and 3).

B. Ionic burst and tail

It is now clear that the competition between the electron impact and the Penning ionizations results in a temporal concentration imbalance of electrons and ions with a microsecond delay in the He-N_2 DBD. It is conceivable that this will be observable also in atmospheric pressure DBD in other gas mixtures, since production of many reactive plasma species is closely related to the electron density and the electron energy.[29] To see this, Fig. 4 shows space-averaged densities of electrons and ions for $[N_2] = 30$ ppm. Helium ions and electrons are seen to reach their maximum concentrations simultaneously during gas breakdown and fall down rapidly, due to the electron impact ionization of He. By contrast, nitrogen ions persist for much longer times, sustaining up to tens of μs, as is consistent with the previous experiment study by a mass/energy analyzer HPR60.[21] Since the electron loss to the wall dominates the electron loss via electron-ion recombination, the plasma becomes positively charged from the gas breakdown. This means that the electrical

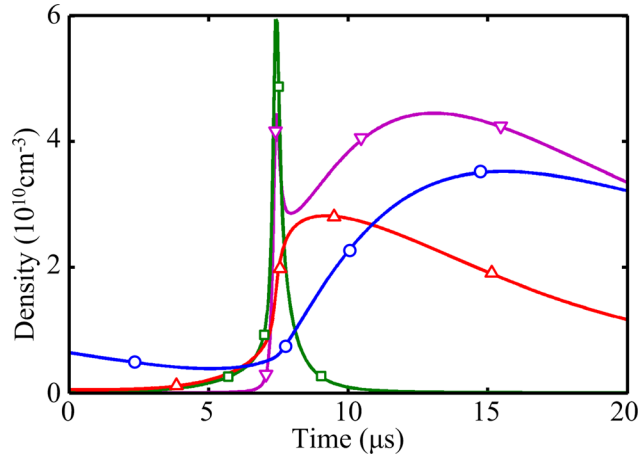

FIG. 4. Space-averaged densities of electrons (–▽–), He_2^+ (–□–), N_2^+ (–△–) and N_4^+ (–○–) as a function of time at $[N_2] = 30$ ppm.

neutrality is broken down right from gas breakdown and well before the nitrogen ions become more abundant than the helium ions. This leads to a train of cation bursts, once every half cycle of the voltage excitation. Breakdown of electrical neutrality is known to be possible in atmospheric pressure plasmas.[28,34]

Fig. 5 shows the temporal profiles of space-averaged electron, ion, and net charge densities. It is evident that the net charge is always positive and so charges in the plasma are characterized by a narrow net positive-charge burst followed by a tail also of net positive charges. The early surge of He_2^+ ions appears to cause the breakdown of the electrical neutrality already and the late surge of nitrogen ions with a larger time- and space-averaged density seems to play a secondary role of maintaining the charge imbalance until the next gas discharge event. Yet nitrogen ions are directly related to production of reactive plasma species and so their role goes beyond contributing to electrical neutrality. For example, important reactive oxygen and nitrogen species such as O, O_2^-, and O_3 may be produced from $N_2^+ + O^- \rightarrow O + N + N$, $N_2^+ + O_3^- \rightarrow O_3 + N + N$, and $N_2^+ + NO^- \rightarrow NO + N_2$. This suggests that reactive plasma species may reach their peak densities at a delayed time similar to the moment of the peak nitrogen ion density when O_2 admixture is included in the plasma-forming gas. This is supported by a recent study of radio-frequency plasma in atmospheric He-O_2 mixture in which electron fluxes are shown to reach an inserted sample before ions.[29,30] Two characters of the He-N_2 DBD are therefore emerging—first a sequence of net positive charge bursts during gas breakdown and second an abundant production of cations and reactive plasma species delayed by a microsecond scale.

Temporal details of ionic and reactive plasma species may impact on some biological processes. For instance, the membrane channel conductance of neuronal cells is known to depend upon how ions are accumulated and released from the cell membrane.[35] Many cell functions including the cell-cell communication and nerve growth are induced by the initiation of the action potential and hence the latter is a key trigger. The axon hillock of a neuron cell has a resting

This article is copyrighted as indicated in the article. Reuse of AIP content is subject to the terms at: http://scitation.aip.org/termsconditions. Downloaded to IP: 117.32.153.177 On: Fri, 19 Sep 2014 02:45:44

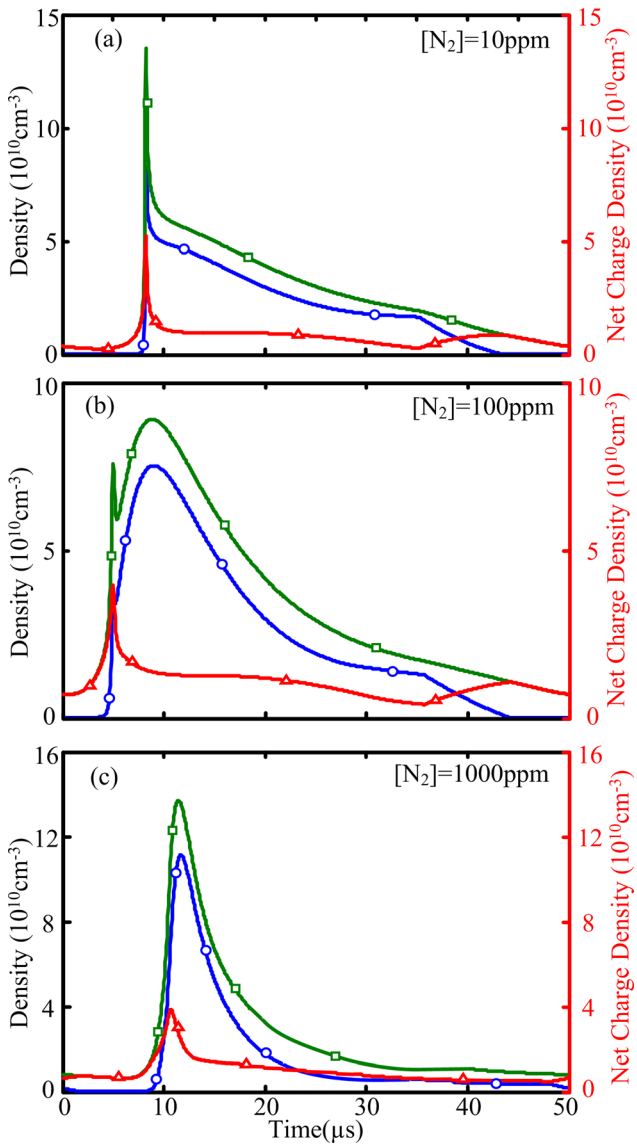

FIG. 5. Space-averaged densities of electron (–○–), ion (–□–) and net charge (–△–) as a function of time.

voltage of about −70 mV and the cell membrane is therefore normally polarized. The negative sign of the membrane voltage indicates that the inside of the membrane is more negatively charged. To initiate the action potential, the membrane needs to be depolarized by increasing the membrane voltage to around −55 mV. This is done usually by injecting extra sodium cations into the cell via several biological mechanisms.[36] Therefore, it is possible to trigger the action potential of neuron cells using the ionic burst of He-N_2 DBD and provide a new idea for some biological processes. Of course, a great deal of work, both in physics and biology, needs to be undertaken before the feasibility is translated into practical therapies.

IV. CONCLUSIONS

A dielectric barrier discharge (DBD) in He-N_2 mixture is studied using a fluid model for temporal characteristics of its chemical species with respect to those of its electric current. It is shown that there exist time delays between the moments of the maximum discharge current density and the maximum space-averaged particle density. The time delays are different with different species, and they change as the volume percentage of N_2 increases. Over the N_2 range up to 10 000 ppm, the time delays for electron, N_2^+, N_4^+, and He_2* are found to depend very strongly on the N_2 content largely due to the competition between the electron impact and Penning ionizations. By contrast, the time delay of the peak He* density to the peak discharge current varies little with increasing N_2 content. Significant electron wall losses lead to the DBD being more positively charged and, with a distinct temporal separation in the peak electron and cation densities, the plasma is characterized with repetitive bursts of net positive charges. The distinct temporal separation in the production of electrons and ionic species stems from different onset times of the competing electron-impact and Penning ionizations, and it is conceivable that a competition of similar or other ionization mechanisms in other plasma systems may lead to pulsed and temporally separated production of charged particles too. The temporal details of ionic and reactive plasma species may provide a new idea for some biological processes.

ACKNOWLEDGMENTS

This work was supported by the National Science Foundation of China (No. 51221005), the State Key Laboratory of Electrical Insulation and Power Equipment (No. EIPE14312).

[1]U. Kogelschatz, IEEE Trans. Plasma Sci. **30**, 1400 (2002).
[2]A. Fridman, A. Chirokov, and A. Gutsol, J. Phys. D: Appl. Phys. **38**, R1 (2005).
[3]S. Kanazawa, M. Kogoma, T. Moriwaki, and S. Okazaki, J. Phys. D: Appl. Phys. **23**, 374 (1990).
[4]D. Z. Pai, G. D. Stancu, D. A. Lacoste, and C. O. Laux, Plasma Sources Sci. Technol. **18**, 045030 (2009).
[5]J. L. Walsh and M. G. Kong, Appl. Phys. Lett. **91**, 251504 (2007).
[6]F. Massines and G. Gouda, J. Phys. D: Appl. Phys. **31**, 3411 (1998).
[7]M. G. Kong, G. Kroesen, G. Morfill, T. Nosenko, T. Shimizu, J. van Dijk, and J. L. Zimmermann, New J. Phys. **11**, 115012 (2009).
[8]J. Genzer and J. Groenewold, Soft Matter **2**, 310 (2006).
[9]V. I. Gibalov and G. J. Pietsch, J. Phys. D: Appl. Phys. **33**, 2618 (2000).
[10]I. Radu, R. Bartnikas, G. Czeremuszkin, and M. R. Wertheimer, IEEE Trans. Plasma Sci. **31**, 411 (2003).
[11]M. G. Kong and X. T. Deng, IEEE Trans. Plasma Sci. **31**, 7 (2003).
[12]R. Dorai and M. J. Kushner, J. Phys. D: Appl. Phys. **34**, 574 (2001).
[13]L. Mangolini, C. Anderson, J. Heberlein, and U. Kortshagen, J. Phys. D: Appl. Phys. **37**, 1021 (2004).
[14]Y. B. Golubovskii and V. A. Maiorov, J. Phys. D: Appl. Phys. **36**, 39 (2003).
[15]X. Yuan, J. Shin, and L. L. Raja, Vacuum **80**, 1199 (2006).
[16]T. Martens and A. Bogaerts, Appl. Phys. Lett. **92**, 041504 (2008).
[17]T. Martens, A. Bogaerts, W. J. M. Brok, and J. van Dijk, Appl. Phys. Lett. **96**, 091501 (2010).
[18]K. Urabe, O. Sakai, and K. Tachibana, J. Phys. D: Appl. Phys. **44**, 115203 (2011).
[19]D. Petrović, T. Martens, J. van Dijk, W. J. M. Brok, and A. Bogaerts, J. Phys. D: Appl. Phys. **42**, 205206 (2009).
[20]Q. Xiong, A. Y. Nikiforov, M. A. Gonzalez, C. Leys, and X. P. Lu, Plasma Sources Sci. Technol. **22**, 015011 (2013).
[21]J. S. Oh, Y. Aranda-Gonzalvo, and J. W. Bradley, J. Phys. D: Appl. Phys. **44**, 365202 (2011).
[22]K. McKay, J. S. Oh, J. L. Walsh, and J. W. Bradley, J. Phys. D: Appl. Phys. **46**, 464018 (2013).
[23]Y. V. Pershin and M. D. Ventra, Adv. Phys. **60**, 145 (2011).

This article is copyrighted as indicated in the article. Reuse of AIP content is subject to the terms at: http://scitation.aip.org/termsconditions. Downloaded to IP: 117.32.153.177 On: Fri, 19 Sep 2014 02:45:44

[24]A. Malmendal, J. Evenas, S. Forsen, and M. Akke, J. Mol. Biol. **293**, 883 (1999).
[25]R. B. Hill, C. Bracken, W. F. DeGrado, and A. G. Palmer, J. Am. Chem. Soc. **122**, 11610 (2000).
[26]E. Z. Eisenmesser, D. A. Bosco, M. Akke, and D. Kern, Science **295**, 1520 (2002).
[27]X. H. Wang, A. J. Yang, M. Z. Rong, and D. X. Liu, Plasma Sci. Technol. **13**, 724 (2011).
[28]A. J. Yang, X. H. Wang, M. Z. Rong, D. X. Liu, F. Iza, and M. G. Kong, Phys. Plasma **18**, 113503 (2011).
[29]D. X. Liu, A. J. Yang, X. H. Wang, M. Z. Rong, F. Iza, and M. G. Kong, J. Phys. D: Appl. Phys. **45**, 305205 (2012).
[30]A. J. Yang, M. Z. Rong, X. H. Wang, D. X. Liu, and M. G. Kong, J. Phys. D: Appl. Phys. **46**, 415201 (2013).
[31]G. J. M. Hagelaar and L. C. Pitchford, Plasma Sources Sci. Technol. **14**, 722 (2005).
[32]H. W. Ellis and R. Y. Pai, At. Data Nucl. Data Tables **17**, 177 (1976).
[33]T. Martens, W. J. M. Brok, J. van Dijk, and A. Bogaerts, J. Phys. D: Appl. Phys. **42**, 122002 (2009).
[34]J. J. Shi and M. G. Kong, Phys. Rev. Lett. **96**, 105009 (2006).
[35]A. L. Hodgkin and A. F. Huxley, J. Physiol. **117**, 500 (1952).
[36]P. G. Kostyuk, N. S. Veselovsky, and A. Y. Tsyndrenko, Neuroscience **6**, 2423 (1981).

This article is copyrighted as indicated in the article. Reuse of AIP content is subject to the terms at: http://scitation.aip.org/termsconditions. Downloaded to IP: 117.32.153.177 On: Fri, 19 Sep 2014 02:45:44